ISSN 1846-6168 (Print), ISSN 1848-5588 (Online)
https://doi.org/10.31803/tg-20250414132406

Original scientific paper
Received: 2025-04-14, Accepted: 2025-06-23

Modelling the Effects of Grinding Wheel Parameters on Surface Roughness during Grinding of D2 Steel

Aleksandar Milosevic, Goran Simunovic, Vitalii Ivanov, Mario Sokac, Vladimir Kocovic, Milana Ilic Micunovic, Djordje Vukelic*

Abstract: The research focused on the effects of abrasive type, grain size, and wheel structure on surface roughness during external cylindrical longitudinal grinding of D2 steel. Experimental research was conducted using a full factorial design. The measured surface roughness values, depending on the combination of input parameters, ranged from 0.22 to 1.31 μm, corresponding to ISO roughness grades N4 to N7. Among the factors examined, grain size had the most significant impact on surface roughness, followed by the type of abrasive, while the grinding wheel structure had the least effect. The best surface roughness is obtained by utilizing corundum with the highest aluminium oxide content as an abrasive, along with the smallest grain size and a dense structure of the grinding wheel. Additionally, modelling of the grinding process was performed. The validity of the obtained regression equation for predicting surface roughness was confirmed through five additional verification experiments, which supported the accuracy of the modelling.

Keywords: abrasive type; grain size; grinding; structure

1 INTRODUCTION

In manufacturing, grinding has many applications, such as finishing, slitting, parting, descaling, deburring, sharpening, etc. Grinding is a crucial finishing operation that ensures high dimensional accuracy and high surface quality. This process allows for the machining of workpieces high accuracy and precision [1]. However, grinding is complex, influenced by numerous factors and their interactions, including the type of grinding, the machine tools, the grinding wheel, fixtures, and grinding parameters [2]. For successful grinding, it is essential to address all these influencing factors [3]. Additionally, grinding can effectively process workpieces made from various materials, each with distinct mechanical, physical, and thermal properties [4]. One such material is D2 steel, which is known for its high wear resistance and good corrosion resistance. However, it presents challenges during machining, especially after heat treatment, as it becomes significantly harder.

In recent years, the grinding of D2 steel has been examined from various perspectives. Karabelchtchikova et al. [5] developed a mathematical model to describe the effects of multipass grinding on residual stress distribution. This model aids in predicting grinding dynamics and the impact of grinding on material characteristics. Mohanasundararaju et al. [6] utilized response surface methodology to predict surface roughness. Their experiments, conducted on a transverse grinding machine, revealed that surface roughness improves with increasing wheel speed, work speed, and dress depth. In contrast, surface roughness decreases with lower traverse speed and feed rate. Yan et al. [7] explored how grinding parameters and wheel grain size influence the formation of white layers. They found that a finer grain size of the wheel makes it more likely for both white and dark layers to form. Additionally, the occurrence of these layers is more probable with increased wheel rotation speed, workpiece speed, and depth of cut. Prabhu and Vinayagam [8] analysed changes in fractal dimension based on the smoothness of the ground surface. They measured surface roughness for carbon nanotube-based nanofluids during the grinding process. Kamely et al. [9] modelled the surface roughness of the grinding process based on feed and working speed. Surface roughness improves as both feed and working speed decrease. Yan et al. [10] developed a finite element simulation model to analyse grinding with alumina abrasive grit. The model assessed material deformation, forces, critical depth of cut, temperature, and material removal rate. Sethuramalingam & Vinayagam [11] studied the effects of grinding parameters using a carbon nanotube-based grinding wheel on surface roughness. They found that cutting speed had the most significant impact on surface roughness, while the depth of cut had the least influence. Babu et al. [12] studied the impact of grinding parameters on surface roughness when carbon nanotubes were added to oil, using the Taguchi method. The findings showed that surface roughness improved with an increase in feed and a decrease in the depth of cut. Khan et al. [13] conducted a comparison of surface quality, surface temperature, and normal force after grinding under three different conditions: dry, wet cooling, and minimum quantity lubrication (MQL). Their findings indicated that MQL outperformed both dry and wet conditions due to its superior penetration ability and enhanced heat dissipation properties. Kannan and Arunachalam [14] examined the relationship between grinding forces and the surface images of ground materials during the dressing process. Their results indicated a strong correlation between the signals from grinding forces and the images of ground surfaces, which can be used to assess the level of wear deterioration. Isti Nugroho et al. [15] examined the characteristics of chips and surface roughness. The results indicated that increasing the feed rate led to greater chip width and higher surface roughness values. Hood et al. [16] studied the performance of electroplated CBN grinding points with varying grit sizes. The most significant factors impacting surface roughness were the number of effective cutting grits and the active area. Gopan et al. [17] examined the effects of table speed, cross-feed, and depth of cut on surface roughness and cutting force. To

reduce surface roughness and cutting force, they utilized artificial neural networks and particle swarm optimization. Ben Fathallah et al. [18] investigated the effects of a sol-gel abrasive wheel and cryogenic cooling on surface integrity. Their study revealed that using a combination of an Al_2O_3 abrasive wheel and soluble oil as a cooling method improved fatigue life when controlled grinding was employed. Chaudhari et al. [19] compared the surface integrity of conventional dry grinding with ultrasonic vibration-assisted dry grinding. The ultrasonic vibration-assisted dry grinding produced less variation in microhardness and resulted in a lower surface roughness. Azami et al. [20] studied the cutting forces and surface roughness during MQL grinding by incorporating MoS_2 and CuO nanoparticles into vegetable-based oils. The addition of these nanoparticles reduced cutting forces and improved surface quality. Chaudhari et al. [21] studied the effect of worktable feed and ultrasonic vibration amplitude on grinding outcomes. A decrease in worktable feed and an increase in ultrasonic vibration lead to reductions in grinding forces, surface roughness, and grinding temperature. Sharma et al. [22] studied grinding forces, specific grinding energy, and surface roughness under dry, wet, and cryogenic conditions. The cryogenic environment reduces grinding forces, lowers specific energy, and improves surface roughness. Mouralova et al. [23] analysed chips after grinding using an Al_2O_3 grinding wheel. They detected four different types of chips post-grinding. Zhang et al. [24] examined how grinding parameters affect surface roughness. Their findings revealed that the surface roughness measured perpendicular to the grinding direction was significantly greater than that measured parallel to it. They also found that increasing the grinding speed or reducing the grinding depth led to a decrease in surface roughness.

The grinding process and its output parameters are influenced by a variety of parameters, many of which are non-linear. Consequently, the success of the grinding process often depends on the operator's experience and expertise. Previous research has typically focused on a few key parameters, including grinding parameters, grinding wheel characteristics, and dressing parameters. To enhance the grinding process, it is essential to model and optimize it by considering as many parameters as possible. This can be achieved by developing appropriate analytical models and identifying optimal grinding conditions.

The objective of this research, unlike previous studies, is to model the process of external cylindrical longitudinal grinding using a straight grinding wheel. Specifically, we aim to develop a mathematical model that includes factors such as abrasive type, grain size, and the structure (porosity) of the grinding wheel. This model will help predict the surface roughness after the grinding operation. Additionally, the study will examine how the grinding wheel factors interact with surface roughness. We also aim to evaluate the impact of each factor and their interactions on the surface roughness. Furthermore, this research seeks to identify and validate, through confirmation experiments, the optimal parameters for the grinding process in order to minimize surface roughness and ensure its repeatability.

2 METHODOLOGY

The methodology according to which the research was conducted consists of several steps (Fig. 1).

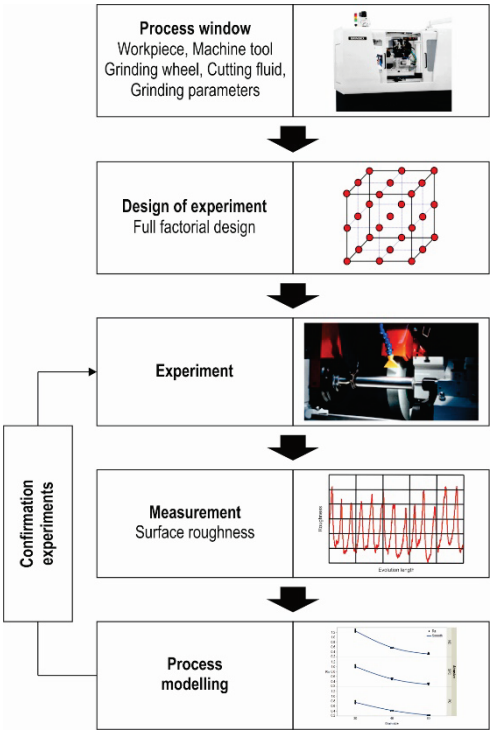

Figure 1 Methodology

Experimental research was conducted on workpieces ∅50 × 350 mm, which had been machined through turning to achieve an initial surface roughness of Ra = 8.3 µm. These workpieces were made from D2 tool steel, which has the following chemical composition: 1.50% Carbon (C), 0.60% Manganese (Mn), 0.60% Silicon (Si), 1.00% Cobalt (Co), 12.00% Chromium (Cr), 1.00% Molybdenum (Mo), 1.10% Vanadium (V), 0.03% Phosphorus (P), 0.30% Nickel (Ni), 0.25% Copper (Cu), 0.03% Sulfur (S), with the balance being Iron (Fe). The key mechanical, physical, and thermal characteristics of D2 tool steel are as follows: Hardness = 62 HRC, Elastic modulus = 200 GPa, Yield strength = 1300 MPa, Poisson's ratio = 0.29, Thermal conductivity = 20 W/m·K, and Thermal expansion = 10.4×10^{-6} 1/°C.

External cylindrical longitudinal grinding was conducted on a grinding machine using the following parameters: a grinding wheel cutting speed of v_c = 25 m/s, a workpiece speed of v_w = 0.2 m/s, a longitudinal feed of f = 25 mm, and a depth of cut of a_p = 0.01 mm. Grinding parameters and the characteristics of the grinding wheel should be selected according to the manufacturer's recommendations.

During external cylindrical grinding, the workpieces are fixed between centers and rotated using the driving plate. The grinding wheel and workpiece rotate in the same direction.

The experiments utilized a grinding wheel with the following dimensions: a diameter of D = 300 mm, a width of T = 50 mm, and a hole diameter of H = 127 mm. Grinding was performed using straight wheels characterized by soft

hardness (designation I) and a ceramic bond type (designation V). During the experimental research, three parameters of the grinding wheels were varied: abrasive type, grain size, and structure (porosity). The levels of the input parameters are detailed in Tab. 1.

Table 1 Parameters of grinding wheels levels

Parameter		Abrasive	Grain size	Structure
Level 1	Designation	Corundum 21A	30	4
	Main characteristic	90 % Al_2O_3	0.710–0.590 μm	Dense
Level 2	Designation	Corundum 41A	46	8
	Main characteristic	94 % Al_2O_3	0.420–0.350 μm	Medium
Level 3	Designation	Corundum 61A	60	12
	Main characteristic	98 % Al_2O_3	0.297–0.250 μm	Very open (porous)

During machining, the synthetic cutting fluid Syntilo 2000 was applied to enhance grinding efficiency. This fluid not only extends tool life but also ensures a high-quality surface roughness and maintains dimensional accuracy.

The experimental research was conducted according to a full factorial design, which allows the investigation of all possible combinations of input parameters. Since all parameters were defined as categorical with three levels each, a total of 27 experimental runs (3×3×3) were conducted.

After conducting experimental research, the measurement of surface roughness, specifically the arithmetical mean roughness value, was conducted using a Mitutoyo surface roughness measuring instrument. The probe tip radius was set at 2 μm, with a sampling length of 0.8 mm and an evaluation length of 4 mm. Measurements were taken at ten different locations on the workpiece, and the average surface roughness value was calculated to aid in model development.

In the final step, we performed an analysis of surface roughness generation and its mathematical modelling using multiple regression analysis. This approach quantifies the relationship between input parameters – such as abrasive type, grain size, and structure – and the response parameter, which is surface roughness. The research employed a full factorial design for the experiments. A mathematical model was created to best fit the measured results, represented as a polynomial with coefficients determined by the measured values of surface roughness. The resulting regression model can be expressed as:

$$Ra = f(x_1, x_2, x_3), \tag{1}$$

where x_1 is abrasive type, x_2 is grain size and x_3 is structure. This leads to the model equation:

$$Ra = \beta + \sum_{i=1}^{3} \beta_i \cdot x_i + \sum_{i=1}^{3} \sum_{j=1}^{3} \beta_{ij} \cdot x_i \cdot x_j + \varepsilon, \tag{2}$$

where β is coefficients and ε is residual.

At the end, using this set of experimental parameters, we identified the conditions that yield the minimum value of surface roughness. We subsequently validated this minimum value through additional confirmation experiments.

3 RESULTS

3.1 Experimental Results

The results of the experiment are shown in Tab. 2. The results were randomized, which reduced the possibility of systematic bias and further increased the reliability of the data obtained.

Table 2 Results of the experiments

No.	Abrasive	Grain size	Structures	*Ra* (μm)
1	21A	46	12	0.58
2	41A	30	12	1.06
3	61A	30	8	0.76
4	61A	30	12	0.80
5	21A	46	8	0.57
6	21A	60	8	0.32
7	61A	46	12	0.43
8	61A	60	4	0.22
9	41A	30	4	0.97
10	41A	30	8	1.01
11	61A	60	12	0.24
12	21A	60	4	0.31
13	61A	30	4	0.71
14	21A	30	4	1.22
15	21A	30	8	1.27
16	61A	46	4	0.41
17	41A	60	12	0.29
18	21A	60	12	0.33
19	41A	46	4	0.48
20	21A	46	4	0.56
21	41A	60	4	0.27
22	61A	46	8	0.42
23	61A	60	8	0.23
24	21A	30	12	1.31
25	41A	46	12	0.51
26	41A	60	8	0.28
27	41A	46	8	0.50

3.2 Statistical Analysis

Statistical analysis of the measured results was conducted using a model that incorporates main effects and two-factor interactions. This approach enabled the development of a model for a detailed investigation and modelling of the complex relationships between input and output parameters.

Due to irregularities observed in the data distribution and significant deviations among individual values (as illustrated in Fig. 2a), a logarithmic transformation of *Ra* (ln (*Ra*)) was applied. This transformation facilitates a better interpretation of the results and the application of statistical methods. The data distribution after the transformation is presented in Fig. 2b.

The logarithmic transformation was chosen based on the findings of a Box-Cox analysis, which indicated an optimal lambda value of $\lambda = -0.13$ (Fig. 3). This value is close to zero, suggesting that a logarithmic transformation is the most suitable option for stabilizing variance and enhancing the

normality of the data. We also assessed other standard transformations, such as square root and reciprocal, but they did not yield better results regarding data distribution or model performance.

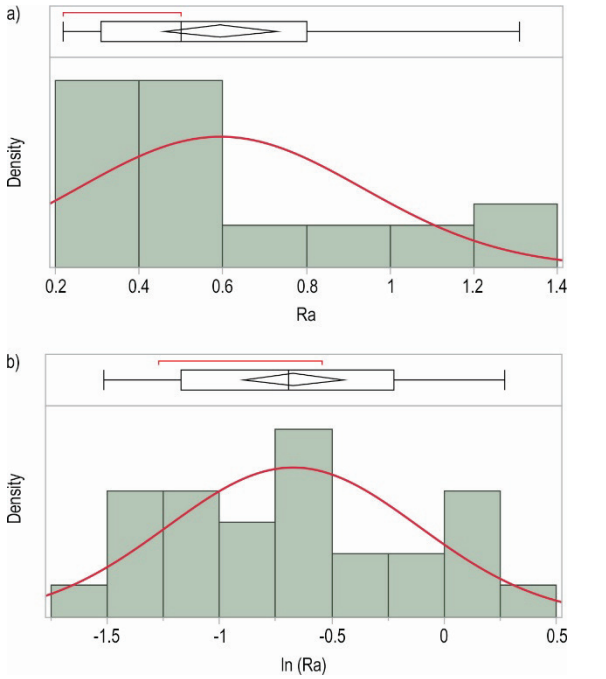

Figure 2 Distribution of surface roughness: a) before transformation b) after transformation

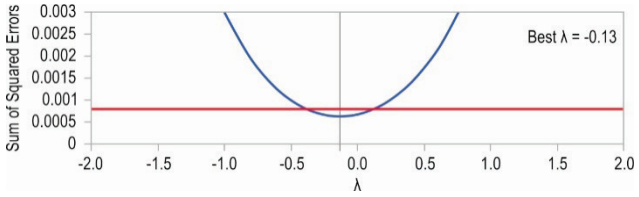

Figure 3 Box-Cox transformation

The assessment of the model's summary of fit predicting the ln (*Ra*) parameter is detailed in Tab. 3. The high coefficient of determination (R^2 = 0.999685) indicates an excellent alignment between the actual and predicted values, with the model accounting for over 99.9% of the total variance in the response parameter. The adjusted coefficient of determination (*Adjusted* R^2 = 0.999489) further verifies the model's reliability, taking into account the number of input parameters used. Additionally, the low root mean square error (*RMSE* = 0.012675), when compared to the mean of the dependent parameter (*Mean of Response* = –0.67167), demonstrates the model's high precision and low average error in its predictions.

Table 3 Summary of fit

Parameter	ln (*Ra*)
R^2	0.999685
R^2 *Adjusted*	0.999489
RMSE	0.012675
Mean of Response	–0.67167

Tab. 4 provides the analysis of variance for the specified regression model. The *F*-ratio obtained is 5085.076, which indicates the statistical significance of the model in explaining the variance of the output parameter. This high *F*-ratio suggests that the model's total effects are significantly greater than the random variations (error). Furthermore, the extremely low *p*-value (< 0.0001) confirms that there is at least one statistically significant effect among the independent parameters. The total sum of squares is 8.1724370, with the model accounting for almost the entire variance (*Sum of Squares Model* = 8.16987), while the error contributes minimally (*Sum of Squares Error* = 0.0025706). This further reinforces the model's effectiveness.

Table 4 Analysis of variance

Source	*DF*	*Sum of Squares*	*Mean Square*	*F Ratio*	*Prob > F*
Model	10	8.1698664	0.816987	5085.076	<0.0001*
Error	16	0.0025706	0.000161		
C. Total	26	8.1724370			
Legend: * - statistically significant ($p < 0.05$, significance threshold)					

Tab. 5 shows the estimated input parameters of the model, ranked based on their LogWorth values. LogWorth represents a measure of the statistical significance of each parameter, with higher values indicating a greater impact of the parameter on the model.

Table 5 Effect summary

Source	*LogWorth*	*p*-value
Grain size	27.693	0.00000
Abrasive	19.331	0.00000
Abrasive×Grain size	8.832	0.00000
Structures	7.988	0.00000

Fig. 4 presents a visual assessment of the model's fit by comparing actual and predicted output parameters. The analysis of this plot reveals a strong alignment between the actual and predicted values, as the points are closely clustered around the diagonal line. This diagonal line signifies the ideal scenario in which predicted values match the actual values, showcasing the model's precision in its predictions.

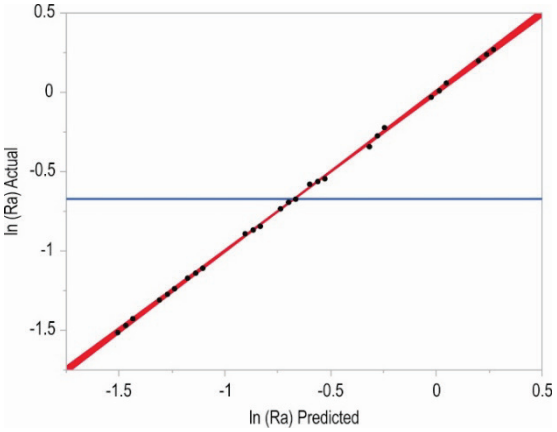

Figure 4 Actual by predicted plot

Fig. 5 displays the residuals plotted against the predicted values. The residuals are evenly distributed around the

horizontal line at zero, showing no obvious patterns. This suggests that the model fits the data well and that there are no systematic trends in the predictions.

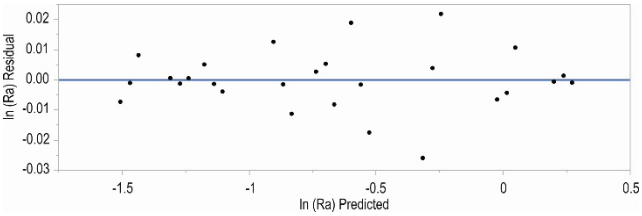

Figure 5 Residual by predicted plot

The normality of the residuals in the model was evaluated using the residuals' normal quantile plot, shown in Fig. 6. The residuals fall within the confidence interval (*CI*) and align with the diagonal line, suggesting that they are normally distributed. Since the points remain within the interval, we can conclude that there are no outliers indicating any irregularities in the data. This plot indicates that the model meets the assumption of normality for the residuals, confirming its validity and ensuring the reliability of the results obtained.

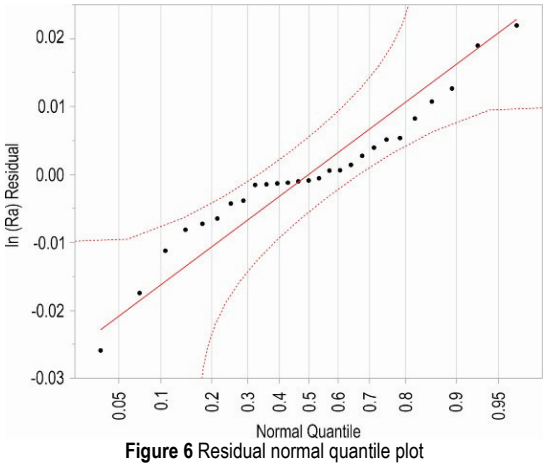

Figure 6 Residual normal quantile plot

Tab. 6 presents the standardized estimates of the regression coefficients regarding the influence of various input parameters on surface roughness. Standardized parameter estimates indicate the relative impact of different input parameters on the dependent parameter, facilitating comparisons irrespective of unit differences. The *Prob>|t|* value reflects the statistical significance of each input parameter, with a value less than 0.005 indicating statistical significance. The t-ratio values demonstrate the relationship between the parameter estimate and its standard error; higher t-ratios signify a stronger influence of the predictor in the model.

Positive and negative estimate values reveal the extent and direction of the effects of individual parameters and their interactions on the output. Positive values for the following parameters - Abrasive [21A], Abrasive [41A], Grit Size [30], Structures [8], Structures [12], Abrasive [21A] × Grain Size [30], Abrasive [41A] × Grain Size [30], Abrasive [41A] × Grain Size [60], Abrasive [61A] × Grain Size [46], and Abrasive [61A] × Grain Size [60] - indicate that applying these parameters increases the ln (Ra) value, which corresponds to a negative effect on the quality of the machined surface.

Table 6 Estimates

Term	Estimate	Std Error	t Ratio	Prob>|t|
Intercept	-0.671666	0.002439	-275.34	<0.0001*
Abrasive [21A]	0.1829939	0.00345	53.05	<0.0001*
Abrasive [41A]	0.0180134	0.00345	5.22	<0.0001*
Abrasive [61A]	-0.201007	0.00345	-58.27	<0.0001*
Grain size [30]	0.6611754	0.00345	191.66	<0.0001*
Grain size [46]	-0.038356	0.00345	-11.12	<0.0001*
Grain size [60]	-0.62282	0.00345	-180.54	<0.0001*
Structures [4]	-0.03657	0.00345	-10.60	<0.0001*
Structures [8]	0.0016314	0.00345	0.47	0.6427
Structures [12]	0.0349391	0.00345	10.13	<0.0001*
Abrasive [21A]×Grain size [30]	0.0634617	0.004879	13.01	<0.0001*
Abrasive [21A]×Grain size [46]	-0.035194	0.004879	-7.21	<0.0001*
Abrasive [21A]×Grain size [60]	-0.028268	0.004879	-5.79	<0.0001*
Abrasive [41A]×Grain size [30]	0.005064	0.004879	1.04	0.3147
Abrasive [41A]×Grain size [46]	-0.008145	0.004879	-1.67	0.1144
Abrasive [41A]×Grain size [60]	0.0030814	0.004879	0.63	0.5366
Abrasive [61A]×Grain size [30]	-0.068526	0.004879	-14.05	<0.0001*
Abrasive [61A]×Grain size [46]	0.0433392	0.004879	8.88	<0.0001*
Abrasive [61A]×Grain size [60]	0.0251865	0.004879	5.16	<0.0001*
Legend: * - statistically significant ($p < 0.05$, significance threshold)				

Through statistical analysis of the chosen model, a regression equation was derived to describe the surface roughness of the machined surface:

$$\begin{aligned}
&\ln(Ra) \\
&= -0.671666049 + Match(Abrasive)\begin{pmatrix} \text{"21A"} & \rightarrow & 0.18299 \\ \text{"41A"} & \rightarrow & 0.01801 \\ \text{"61A"} & \rightarrow & -0.20101 \\ else & \rightarrow & . \end{pmatrix} \\
&\quad + Match(Abrasive)\begin{bmatrix} \text{"21A"} & \rightarrow & Match(Grain\ size)\begin{pmatrix} \text{"30"} & \rightarrow & 0.06346 \\ \text{"46"} & \rightarrow & -0.01352 \\ \text{"60"} & \rightarrow & -0.02827 \\ else & \rightarrow & . \end{pmatrix} \\ \text{"41A"} & \rightarrow & Match(Grain\ size)\begin{pmatrix} \text{"30"} & \rightarrow & 0.00506 \\ \text{"46"} & \rightarrow & -0.00814 \\ \text{"60"} & \rightarrow & 0.00308 \\ else & \rightarrow & . \end{pmatrix} \\ \text{"61A"} & \rightarrow & Match(Grain\ size)\begin{pmatrix} \text{"30"} & \rightarrow & -0.06852 \\ \text{"46"} & \rightarrow & 0.04334 \\ \text{"60"} & \rightarrow & 0.02519 \\ else & \rightarrow & . \end{pmatrix} \end{bmatrix} \\
&\quad + Match(Grain\ size)\begin{pmatrix} \text{"30"} & \rightarrow & 0.66117 \\ \text{"46"} & \rightarrow & -0.03835 \\ \text{"60"} & \rightarrow & -0.62282 \\ else & \rightarrow & . \end{pmatrix} \\
&\quad + Match(Structure)\begin{pmatrix} \text{"4"} & \rightarrow & -0.03657 \\ \text{"8"} & \rightarrow & 0.00163 \\ \text{"12"} & \rightarrow & 0.03494 \\ else & \rightarrow & . \end{pmatrix}
\end{aligned} \tag{3}$$

Fig. 7 shows a statistically significant interaction between abrasive type and grain size in relation to ln (*Ra*). The interaction analysis indicates that the effect of one factor on *Ra* depends on the value of the other factor.

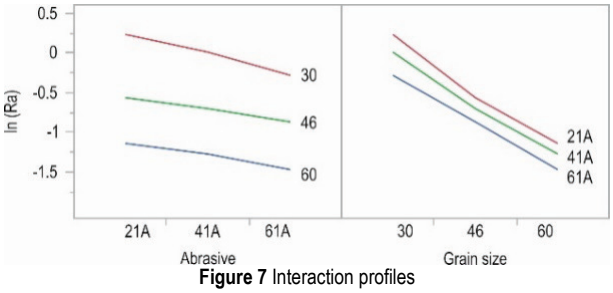

Figure 7 Interaction profiles

Fig. 8 presents the prediction profiler, which illustrates the influence of each input parameter on the predicted surface roughness. The prediction profiler provides insight into how variations in the input parameters affect the output of the regression model.

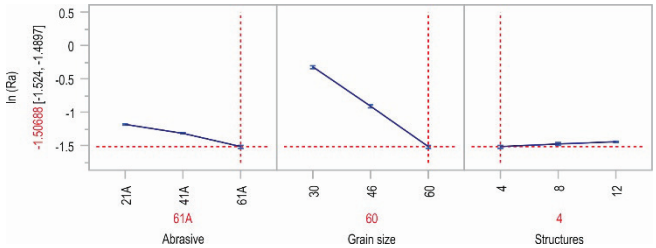

Figure 8 Prediction profiler

3.3 Confirmation Experiments

The regression model was confirmed by 5 additional experiments carried out at the point in the experimental space where the model predicts the lowest *Ra*, i.e. the highest quality of the machined surface. The confirmation experiments were carried out with the following input parameters: abrasive 61A, grain size 60 and structure 4. The experiments were repeated ten times to evaluate the stability and repeatability of the process, and the results obtained were compared with the values predicted by the regression model.

The results of the confirmation experiments are shown in Fig. 9 as box plots. The red horizontal line represents the predicted surface roughness value *Ra* = 0.2216, while the green lines indicate the boundaries of the 95% *CI* (lower *CI* = 0.2178, upper *CI* = 0.2254). The blue line within the box plots connects the mean values of the measurements for each experiment. The obtained results show that both the median and mean fall within the *CI* (95%), indicating the high accuracy and reliability of the developed model, as well as the stability and repeatability of the process. The presence of minor deviations in individual measurements, i.e., statistically acceptable outliers outside the *CI*, can be considered a result of inherent data variability. Based on the obtained results, it can be concluded that the regression model was successfully validated through additional, independent experiments.

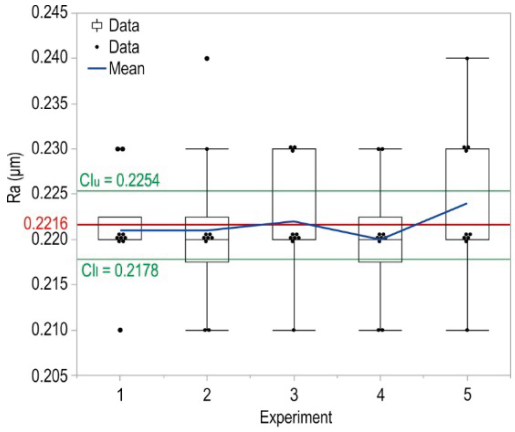

Figure 9 Results of the confirmation experiments

4 DISCUSSION

The results of the statistical analysis and the analysis of variance show a high precision and statistical significance of the developed model. Based on the evaluation of the input parameters, it can be concluded that all main effects as well as the interaction between abrasive type and grain size are statistically significant, while other two-factor interactions are not. The parameter estimation of the developed model showed that grain size and abrasive type are the most influential factors affecting surface roughness.

The greatest effect on *Ra* is attributed to grain size, with a smaller grain size leading to a better surface roughness. Coarse abrasives, which are characterized by larger grain sizes, generate more heat and a rougher surface on the workpiece. In contrast, finer abrasives with smaller grain sizes create multiple contact between the grinding wheel and the workpiece. This results in a more uniform scratch pattern, reduces the peak-to-valley height and ultimately improves the surface roughness.

The best surface quality was achieved with the abrasive 61A, which contains the highest proportion of aluminium oxide, while the poorest quality was achieved with the abrasive 21A, which has the lowest aluminium oxide content. As the aluminium oxide content in abrasives increases, the hardness of the abrasive also increases. This leads to slower wear, which ultimately improves the surface roughness. In addition, abrasives with a higher aluminium oxide content are more resistant to stress, which ensures more even wear and further improves the quality of the machined surface.

The grinding wheel with dense structure showed a better surface quality compared to medium and porous structure. Reducing the porosity of the grinding wheel (fewer pores) increases the contact area between the wheel and the workpiece. This can lead to higher contact pressures and forces as well as insufficient heat dissipation in the cutting zone, which can result in poorer surface roughness. However, careful selection of grinding parameters combined with adequate cooling and lubrication can mitigate these negative effects. In addition, grinding wheels with lower porosity provide less space for the accumulation of chips (dust particles), which can further hinder the achievement of the desired surface roughness. Nevertheless, properly aligned coolant nozzles and adequate coolant pressure can effectively flush the cutting zone and remove chips. Grinding wheels with lower porosity also tend to wear more slowly. Therefore, a wheel with lower porosity can only slightly improve the surface roughness.

The statistically significant interaction between abrasive type and grain size revealed that smaller grain sizes result in reduced surface roughness, regardless of the abrasive used. However, the extent of this improvement varies depending on the abrasive type. The highest surface roughness was recorded for the combination of 21A abrasive and grain size 30, while the lowest roughness was achieved using 61A abrasive with grain size 60.

Visual evaluation of model performance through actual by predicted, residual by predicted, and residual normal quantile plots showed no presence of systematic errors, improper residual distribution, or deviation from normality. The results of confirmation experiments demonstrated high

model accuracy. The predicted and actual values match within the 95% *CI*, further confirming the validity of the developed model and its capability to reliably predict surface roughness.

5 CONCLUSION

The results of the experimental research indicated that the input parameters significantly influence surface roughness. Specifically, surface roughness values varied from 0.22 μm to 1.31 μm. Among the factors studied, grain size had the most substantial effect on surface roughness, while the structure of the grinding wheel had the least impact. Additionally, the interaction between abrasive type and grain size also significantly affected surface roughness.

The results from the statistical analysis and confirmation experiments demonstrated that it is indeed possible to model surface roughness accurately and precisely based on the type of abrasive, grain size, and structure. This conclusion is supported by the fitting parameters obtained and the residuals that were analysed.

The conducted research has certain limitations that can guide future studies. The results obtained are applicable only within the specific conditions under which the experiments were conducted. To enhance the generalizability of the developed model, we plan to conduct experimental research on specimens with varying mechanical, physical, and thermal properties, as well as tools that have different geometric and technological characteristics. Additionally, future research will focus on modelling and optimizing a greater number of variables. This includes incorporating a wider range of input parameters, such as wheel speed, workpiece speed, feed rate, total depth of cut, and the number of passes, along with various output process parameters like dimensional accuracy, material removal rate, hardness, and residual stresses. We also intend to explore other modelling and optimization methods. Finally, future research will investigate wear mechanisms, chip morphology, and related factors.

6 REFERENCES

[1] Kishore, K., Sinha, M. K., Singh, A., Archana, Gupta, M. K., & Korkmaz, M. E. (2022). A comprehensive review on the grinding process: Advancements, applications and challenges. *Proceedings of the Institution of Mechanical Engineers, Part C: Journal of Mechanical Engineering Science, 236*(22), 10923–10952. https://doi.org/10.1177/09544062221110782

[2] Trung, D. D. (2021). Influence of Cutting Parameters on Surface Roughness in Grinding of 65G Steel. *Tribology in Industry*, 43(1), 167–176. https://doi.org/10.24874/ti.1009.11.20.01

[3] Buchmeister, B., Palcic, I., Ojstersek, R., Kovic, K., & Javernik, A. (2024). Multicriteria Optimisation of Machining Operations Using a Spreadsheet Model. *Tehnicki glasnik – Technical Journal, 18*(3), 445–451. https://doi.org/10.31803/tg-20240514150731

[4] Saric, T., Simunovic, G., Vukelic, D., Simunovic, K., & Lujic, R. Estimation of CNC Grinding Process Parameters Using Different Neural Networks. (2018). *Tehnicki Vjesnik – Technical Gazette, 25*(6), 1770–1775. https://doi.org/10.17559/tv-20180419095119

[5] Karabelchtchikova, O., Rivero, I. V., & Hsiang, S. M. (2008). Modeling of residual stress distribution in D2 steel via grinding dynamics using a second-order damping system. *Journal of Materials Processing Technology, 198*(1–3), 313–322. https://doi.org/10.1016/j.jmatprotec.2007.07.006

[6] Mohanasundararaju, N., Sivasubramanian, R., & Alagumurthi, N. (2008). Optimisation of work roll grinding using Response Surface Methodology and evolutionary algorithm. *International Journal of Manufacturing Research, 3*(2), 236. https://doi.org/10.1504/ijmr.2008.017418

[7] Yan, L., Jiang, F., & Rong, Y. M. (2011). Experimental Study on Microstructure Evolution in AISI D2 Steel Surface Grinding. *Key Engineering Materials*, 487, 126–130. https://doi.org/10.4028/www.scientific.net/kem.487.126

[8] Prabhu, S., & Vinayagam, B. K. (2011). Fractal dimensional surface analysis of AISI D2 Tool steel material with nanofluids in grinding process using atomic force microscopy. *Journal of the Brazilian Society of Mechanical Sciences and Engineering, 33*(4), 459–466. https://doi.org/10.1590/s1678-58782011000400009

[9] Kamely, M.A., Kamil, S.M., & Chong C.W. (2011). Mathematical modeling of surface roughness in surface grinding operation. *World Academy of Science, Engineering and Technology*, 80, pp. 1048–1051.

[10] Yan, L., Jiang, F., & Fang, C. F. (2014). Research on Material Removal Mechanism of Single Grit Cutting Based on FEM Simulation. *Advanced Materials Research*, 1017, 82–87. https://doi.org/10.4028/www.scientific.net/amr.1017.82

[11] Sethuramalingam, P., & Vinayagam, B. K. (2016). Multi Objective Optimization of Multi Wall Carbon Nanotube Based Nanogrinding Wheel Using Grey Relational and Regression Analysis. *Journal of the Institution of Engineers (India): Series C*, 97(3), 407–416. https://doi.org/10.1007/s40032-016-0238-9

[12] Babu, O. S., Mamilla, V. R., & Lakshmi Narayana Rao, G. (2016). Finite Element Analysis of Surface Grinding Process Using Nanofluids. Innovative Design and Development *Practices in Aerospace and Automotive Engineering*, 169–174. https://doi.org/10.1007/978-981-10-1771-1_21

[13] Khan, A. M., Jamil, M., Mia, M., Pimenov, D. Y., Gasiyarov, V. R., Gupta, M. K., & He, N. (2018). Multi-Objective Optimization for Grinding of AISI D2 Steel with Al_2O_3 Wheel under MQL. *Materials, 11*(11), 2269. https://doi.org/10.3390/ma11112269

[14] Kannan, K., & Arunachalam, N. (2018). Grinding wheel redress life estimation using force and surface texture analysis. *Procedia CIRP*, 72, 1439–1444. https://doi.org/10.1016/j.procir.2018.03.031

[15] Isti Nugroho, W., Nugroho, S., & Rusnaldy. (2018). Characterization chip formation of commercial steel materials at low speed cylindrical grinding processes. *MATEC Web of Conferences*, 159, 02023. https://doi.org/10.1051/matecconf/201815902023

[16] Hood, R., Medina Aguirre, F., Soriano Gonzalez, L., Novovic, D., & Soo, S. L. (2019). Evaluation of superabrasive grinding points for the machining of hardened steel. *CIRP Annals, 68*(1), 329–332. https://doi.org/10.1016/j.cirp.2019.04.090

[17] Gopan, V., Wins, K. L. D., Evangeline, G., & Surendran, A. (2020). Experimental Investigation for the Multi-objective Optimization of Machining Parameters on AISI D2 Steel Using Particle Swarm Optimization Coupled with Artificial Neural Network. *Journal of Advanced Manufacturing Systems, 19*(03), 589–606. https://doi.org/10.1142/s0219686720500286

[18] Ben Fathallah, B., Braham, C., & Sidhom, H. (2020). Combined effects of abrasive type and cooling mode on fatigue

resistance of AISI D2 ground surface. *International Journal of Fatigue*, 138, 105665. https://doi.org/10.1016/j.ijfatigue.2020.105665

[19] Chaudhari, A., Sharma, A., Awale, A. S., Yusufzai, M. Z. K., & Vashista, M. (2021). Effect of ultrasonic vibration assisted dry grinding on hysteresis loop characteristics of AISI D2 tool steel. *Sadhana, 46*(4), 245. https://doi.org/10.1007/s12046-021-01771-5

[20] Azami, A., Salahshournejad, Z., Shakouri, E., Sharifi, A. R., & Saraeian, P. (2023). Influence of nano-minimum quantity lubrication with MoS2 and CuO nanoparticles on cutting forces and surface roughness during grinding of AISI D2 steel. *Journal of Manufacturing Processes*, 87, 209–220. https://doi.org/10.1016/j.jmapro.2023.01.029

[21] Chaudhari, A., Sharma, A., Yusufzai, M. Z. K., & Vashista, M. (2023). The grindability performance and measurement of surface functional parameter capabilities of difficult-to-machine tool steel under tangential ultrasonic-vibration-assisted dry grinding. *Machining Science and Technology*, 27(3), 268–291. https://doi.org/10.1080/10910344.2023.2224856

[22] Sharma, A., Chaudhari, A., Yusufzai, M. Z. K., & Vashista, M. (2024). Effectiveness of using liquid nitrogen cryogen in grinding to enhance the grinding performance of hard steel. *Proceedings of the Institution of Mechanical Engineers, Part B: Journal of Engineering Manufacture*, 238(1–2), 315–327. https://doi.org/10.1177/09544054221147622

[23] Mouralova, K., Zahradnicek, R., Benes, L., & Fries, J. (2024). Analysis of spherical chips after grinding. *Measurement*, 229, 114401. https://doi.org/10.1016/j.measurement.2024.114401

[24] Zhang, T., Wang, Q., Wang, N., Yan, L., Jiang, F., Zhang, E., Zhou, W., Gao, H., & Wang, Y. (2025). Surface Integrity in the Grinding of Hardened AISI D2 Steel. *Materials, 18*(4), 814. https://doi.org/10.3390/ma18040814

Authors' contacts:

Aleksandar Milosevic
University of Novi Sad, Faculty of Technical Sciences,
Trg Dositeja Obradovica 6, 21000 Novi Sad, Serbia

Goran Simunovic
University of Slavonski Brod, Mechanical Engineering Faculty,
Trg Ivane Brlic Mazuranic 2, 35000 Slavonski Brod, Croatia

Vitalii Ivanov
Sumy State University, Faculty of Technical Systems and Energy Efficient Technologies,
Rymskogo-Korsakova 2, 40007 Sumy, Ukraine

Mario Sokac
University of Novi Sad, Faculty of Technical Sciences,
Trg Dositeja Obradovica 6, 21000 Novi Sad, Serbia

Vladimir Kocovic
University of Kragujevac, Faculty of Engineering,
Sestre Janjic 6, 34000 Kragujevac, Serbia

Milana Ilic Micunovic
University of Novi Sad, Faculty of Technical Sciences,
Trg Dositeja Obradovica 6, 21000 Novi Sad, Serbia

Djordje Vukelic
(Corresponding author)
University of Novi Sad, Faculty of Technical Sciences,
Trg Dositeja Obradovica 6, 21000 Novi Sad, Serbia
E-mail: vukelic@uns.ac.rs